On the use of Galerkin-Eckhaus method to study the nonlinear regime of Marangoni-Bénard instabilities in an evaporating liquid layer

J. Margerit,[*] M. Dondlinger and P.C. Dauby

Université de Liège, Institut de Physique B5a,
Allée du 6 Août 17, B-4000 Liège, Belgium

September 18, 2006

Abstract

We investigate theoretically Marangoni-Bénard instability in an evaporating liquid layer surmounted by its vapor and an inert gas. A Galerkin-Eckhaus method, based on a slaving principle and an iterative algorithm, and a direct finite element method are used to determine the evaporation rate above the convective threshold. Both methods provide precise quantitative results, even far from the linear stability threshold.

Keywords: Marangoni convection; Evaporation; Pattern formation; Amplitude equations

---

[*]Corresponding author. *E-mail address:* jonathan.margerit@ulg.ac.be

1 Introduction

Evaporative convection plays an important role in heat exchangers, distillation columns, and drying technologies. Indeed, if the liquid is volatile enough, the latent heat consumption caused by evaporation at the interface can lead to a vertical temperature gradient which is sufficient to induce an instability. The thermoconvective motion that appears gives rise to an increase of the evaporation rate and of the heat exchange between the liquid and the outside of the system. Arrangements of hexagons, rolls or square convective patterns are then observed [1, 2, 3].

In this paper we consider a pure liquid layer that evaporates in an inert gas. Moreover, we consider a not saturated vapor–gas mixture, i.e., a small vapor mass fraction is imposed at the top of the gas layer, so that liquid evaporation is induced and the gas is pumped at the top of this layer to maintain a constant thermodynamical pressure. Due to evaporation, the liquid depth decreases in the course of time and the motionless liquid reference state is time dependent. However, thanks to the usually large value of the latent heat of vaporization of the liquid, the time evolution of the perturbations is much faster than the displacement of the liquid free surface and it has been shown [4] that this basic solution can be frozen during the stability analysis.

The theoretical linear stability analysis of this problem is well documented when the interface can be considered as nondeformable, which is actually the case when the liquid depth is not too small [5, 6, 2, 7, 8]. The role of interfacial deformations on the linear stability threshold has been examined by Moussy et al. [9] for the same free boundary problem, and also recently by Borcia et al. [10] in the framework of a phase field model and for the case of a liquid that evaporates in its own vapor.

Above the linear stability threshold, a weakly nonlinear stability analysis has been

carried out by Dondlinger et al. [11] and Margerit et al. [12] for the nondeformable configuration, and by Sultan et al. [13] for the additional case of a thin film within the lubrification theory framework. All these nonlinear studies assume that the gas layer is *passive*, i.e., that the evaporation rate remains small enough for convection in the gas to be negligible, and it was verified that the gas conductivity can also be neglected in general, because the ratio of the gas to liquid conductivities is small**: these hypotheses define the so-called 1.5-sided model, which was introduced in [12], and consists of the liquid layer equations plus the needed diffusion equation for the vapor in the gas to account for evaporation. This description proved to improve noticeably the simple one-sided evaporation model [14] that consists of the classical Marangoni-Bénard liquid layer equations with a constant Biot number that artificially takes care of evaporation**. Note that Ozen and Narayanan [15] have recently **get rid of the passive gas layer assumption by considering** the whole two-layer weakly nonlinear solution**, i.e. the two-sided model,** but for the particular configuration of a liquid that evaporates in its own vapor in two-dimensional space.

The purpose of the present work is to determine the evaporation rate **of the 1.5-sided model** as a function of the distance to threshold **in the nonlinear regime**. ~~The motion of the gas phase will be neglected but the mass diffusion equation in the gas phase will be taken into account in the present paper: these hypotheses define the so-called 1.5-sided model which was introduced in [12].~~ Our approach will ~~also~~ be restricted to two dimensional situations **with no amplitude spatial modulation [16]**.

To analyze the behavior of the system above the linear stability threshold, we will use the Galerkin-Eckauss method (GEM) and compare its predictions with purely numerical simulations. This method has already been considered in [11, 12], but with the restriction that only the evolution of the critical modes was considered. For this reason, the solu-

tions were asymptotically correct only close to the threshold and the stability diagrams presented in these papers are only qualitative results. To obtain quantitative predictions even far above the stability threshold, we will extend the GEM and deduce amplitude equations for a larger set of modes, which is determined using an iterative algorithm that was developed by Dauby et al. [17].

The structure of the paper is the following. In Section 2, the physical system, the set of governing equations, and some dimensionless physical parameters are introduced. Section 3 deals with the different numerical techniques that we have used to solve the 1.5-sided model and Section 4 is devoted to the comparison between these methods. Finally, conclusions are drawn in Section 5.

2   Problem formulation

We consider an evaporating liquid layer of infinite horizontal extent and depth d_l, surmounted by a gas layer of thickness d_g (Fig. 1). The gas layer is a mixture of an inert gas and the vapor of the liquid.

The lower, rigid and perfectly heat-conducting plate is maintained at the temperature T_e. At the upper surface of the gas layer, the vapor mass fraction and the thermodynamic pressure are assumed to be fixed at the respective $Y_{v,e}$ and P_e values. Similarly, the temperature of this surface is also maintained at a fixed value which is equal to the temperature T_e imposed at the bottom of the system. We assume that the Boussinesq approximation is valid, that the gas may be taken as perfect, and that local thermodynamic equilibrium is achieved at the liquid-gas interface [8, 7]. The interface is assumed to be nondeformable and the slow decrease of the liquid thickness due to evaporation is neglected since the latent heat of vaporization is large. **Since the interface velocity**
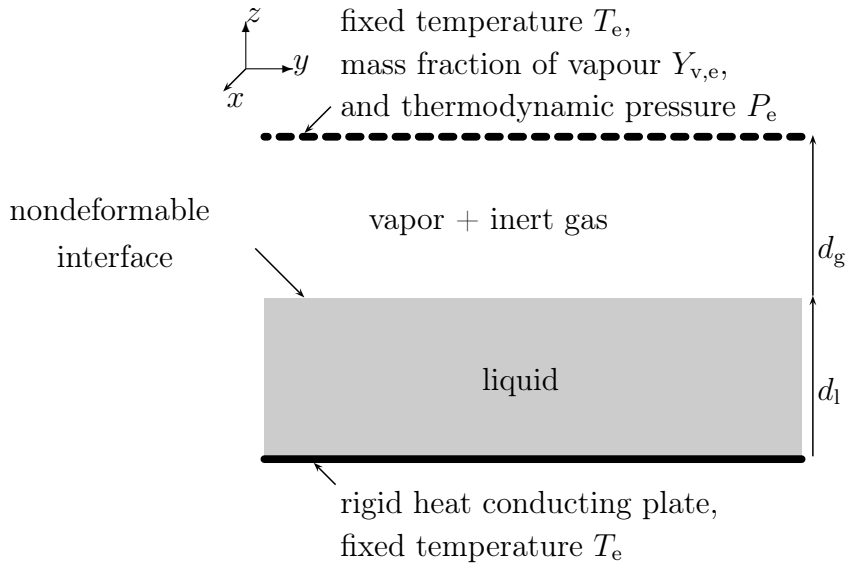
4

Figure 1: System under study.

is the opposite of the evaporation rate [4, 12] due to mass conservation, this leads moreover to a zero vertical velocity of the liquid at the interface.

This evaporation problem has a basic conductive reference state characterized by liquid at rest. The dimensionless velocity, temperature, vapor mass fraction fields, and evaporation rate are respectively given by

$$\mathbf{V}_{\mathrm{ref}} = 0, \tag{1a}$$

$$T_{\mathrm{ref}} = (T_{\mathrm{ref,i}} - T_{\mathrm{e}})z + T_{\mathrm{e}}, \tag{1b}$$

$$Y_{\mathrm{v,ref}} = \frac{Y_{\mathrm{v,ref,i}} - Y_{\mathrm{v},t}}{1 - H}(z - H) + Y_{\mathrm{v},t}, \tag{1c}$$

$$J_{\mathrm{ref}} = T_{\mathrm{e}} - T_{\mathrm{ref,i}}, \tag{1d}$$

where the non dimensional thickness of the system is given by $H = 1 + d_{\mathrm{g}}/d_{\mathrm{l}}$; subscripts ref and i describe respectively the basic (and conductive) reference

state and the liquid-gas interface while $T_{\mathrm{ref,i}}$ and $Y_{\mathrm{v,ref,i}}$ are respectively the dimensionless temperature and vapor mass fraction at the interface in the basic reference state. These two quantities are functions of the temperature T_{e} and are obtained numericaly by resolution of a three algebraic equation system for the three unknowns $T_{\mathrm{ref,i}}$, $Y_{\mathrm{v,ref,i}}$ and J_{ref} [6, 11, 12], system that relies on evaporation laws.

To study the stability of this basic conductive reference state, small perturbations $(\mathbf{v} = (u, v, w), \pi, \theta, y_{\mathrm{v}}, j)$ for the velocity, pressure, temperature, vapor mass fraction, and evaporation rate respectively are introduced. Under rather general assumptions which were determined in details in [12], the 1.5-sided model can be derived and the corresponding dimensionless equations and boundary conditions governing the system are the following:

for $0 \leq z \leq 1$:

$$\nabla \cdot \mathbf{v} = 0, \tag{2}$$

$$\partial_t \mathbf{v} + \mathbf{v} \cdot \nabla \mathbf{v} + \nabla \pi - \mathrm{Pr} \nabla^2 \mathbf{v} = 0, \tag{3}$$

$$\partial_t \theta + \mathbf{v} \cdot \nabla \theta + (T_{\mathrm{ref,i}} - T_{\mathrm{e}}) w - \nabla^2 \theta = 0, \tag{4}$$

for $1 \leq z \leq H$:

$$\partial_t y_{\mathrm{v}} - \frac{\kappa}{\mathrm{Le}} \nabla^2 y_{\mathrm{v}} = 0, \tag{5}$$

at $z = 0$:

$$\mathbf{v} = \theta = 0, \tag{6}$$

at $z = H$:

$$y_{\mathrm{v}} = 0, \tag{7}$$

and at $z = 1$:

$$w = 0, \tag{8}$$

$$\partial_z u + \mathrm{Ma}\partial_x \theta = 0,$$

$$\partial_z v + \mathrm{Ma}\partial_y \theta = 0, \tag{9}$$

$$-\partial_z \theta = j, \tag{10}$$

$$y_{\mathrm{v}} = Y_{\mathrm{i}}(T_{\mathrm{ref,i}} + \theta) - Y_{\mathrm{i}}(T_{\mathrm{ref,i}}), \tag{11}$$

$$j = \frac{J_{\mathrm{ref}}y_{\mathrm{v}} - \frac{\rho\kappa}{\mathrm{Le}}\partial_z y_{\mathrm{v}}}{1 - Y_{\mathrm{v,ref,i}} - y_{\mathrm{v}}}. \tag{12}$$

with Pr and Ma respectively the Prandtl and Marangoni numbers; Le is Lewis number, i.e., the ratio of the heat and mass diffusivities of the gas; ρ and κ are the gas to liquid density and heat diffusivity ratios. ~~The non-dimensional thickness of the system is given by $H = 1 + d_{\mathrm{g}}/d_{\mathrm{l}}$; subscripts ref and i describe respectively the basic (and conductive) reference state and the liquid-gas interface while $T_{\mathrm{ref,i}}$, $Y_{\mathrm{v,ref,i}}$, and J_{ref} are respectively the temperature at the interface, the vapor mass fraction at the interface, and the evaporation rate in the basic reference state.~~ The function $Y_{\mathrm{i}}(T)$ is given by

$$Y_{\mathrm{i}}(T_{\mathrm{l}}) = [1 - r_{\mathrm{w}} + r_{\mathrm{w}}\frac{P_{\mathrm{e}}}{p_{\mathrm{sat}}(T_{\mathrm{l}})}]^{-1}, \tag{13}$$

where $p_{\mathrm{sat}}(T)$ gives the non dimensional pressure as a function of T along liquid-vapor saturation curve; r_{w} is the ratio of the inert gas and liquid molecular weights.

For the results presented in the present paper, the case of water evaporating in air

is considered. A microgravity environment is assumed and the pressure of the air is 1 atmosphere. The vapor mass fraction at the top plate is fixed to zero and the thicknesses of the layers are $d_l = 0.3$ mm and $d_g = 10$ mm. Moreover all physical properties of the fluids are evaluated at the temperature T_e which is the control parameter of our study. We have verified in [12] that those physical and geometrical conditions are within the validity domain of the 1.5-sided model. The critical temperature defining the instability threshold is given by $T_{e,c} = 316.541$ K and the corresponding critical wavenumber is $k_c = 1.956$.

As T_e is the control parameter of our study, it is natural to define the relative distance to the linear stability threshold by $\varepsilon = T_e/T_{e,c} - 1$. This definition of the bifurcation control parameter ε is very convenient but not standard among the thermoconvection community. Indeed, the usual bifurcation control parameter ε_p is rather defined in terms of the temperature difference $\Delta T_{ref} = T_e - T_{ref,i}$ between the bottom plate and the liquid interface. One has $\varepsilon_p = \Delta T_{ref}/\Delta T_{ref,c} - 1$, where subscript c describes the critical conditions. ΔT_{ref} is of course a function of the temperature T_e ~~that can be derived directly from the basic reference evaporative solution that is obtained numericaly by resolution of a three algebraic equation system [11, 12]~~. In Fig. 2, ΔT_{ref}, $T_{ref,i}$, **and** $Y_{v,ref,i}$ are plotted against the bottom plate temperature difference $T_e - T_{e,c}$.

It is important to note that the temperature difference across the liquid layer is much smaller than temperature difference $T_e - T_{e,c}$ imposed at the bottom plate. For this reason, the variations with the temperature T_e of the different physical properties of the fluid must be taken into account. In the classical Marangoni-Bénard problem without evaporation [18] those variations are always negligible, and the present problem is thus a bit more delicate. It is also interesting to plot both bifurcation parameters ε and ε_p against $T_e - T_{e,c}$. Figure 3 shows that ε_p is always much larger than ε so that the notion of distance to the **linear stability** threshold must be considered with caution if one

8

wants to compare our nonlinear results with those corresponding to the more classical Marangoni-Bénard problem without evaporation.
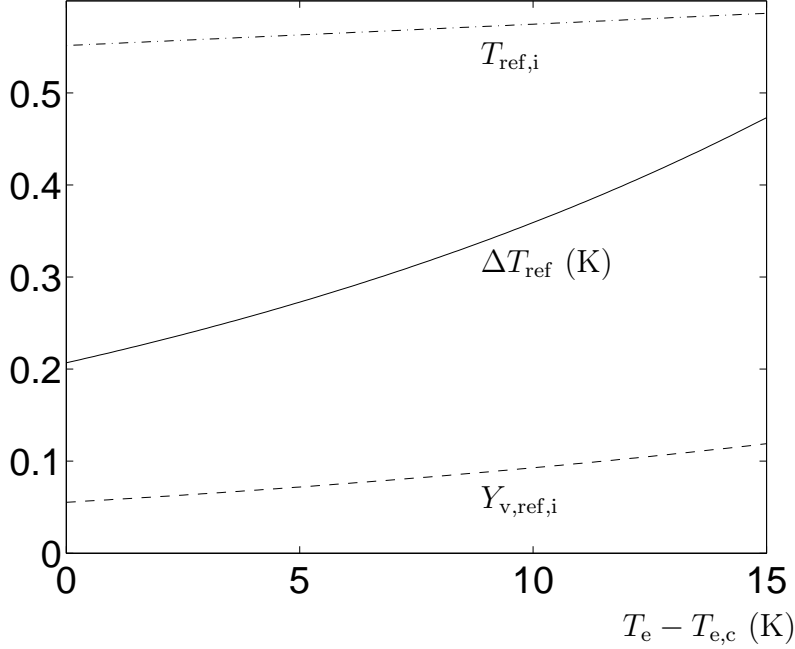

Figure 2: Temperature difference across the liquid layer, $T_{\text{ref,i}}$, **and** $Y_{\text{v,ref,i}}$ (reference state) as a function of $T_{\text{e}} - T_{\text{e,c}}$.

To study the nonlinear regime, it is appropriate to rewrite Eqs. (2)–(13) in terms of linear and nonlinear operators as follows:

$$L_{\varepsilon}f = M\partial_t f + N(f), \tag{14a}$$

$$Bf = 0, \tag{14b}$$

where

$$f^{\text{T}} = (\mathbf{v}, \pi, \theta, y_{\text{v}}, u\mid_{z=1}, v\mid_{z=1}, \theta\mid_{z=1}, \partial_z y_{\text{v}}\mid_{z=1}), \tag{15}$$

9
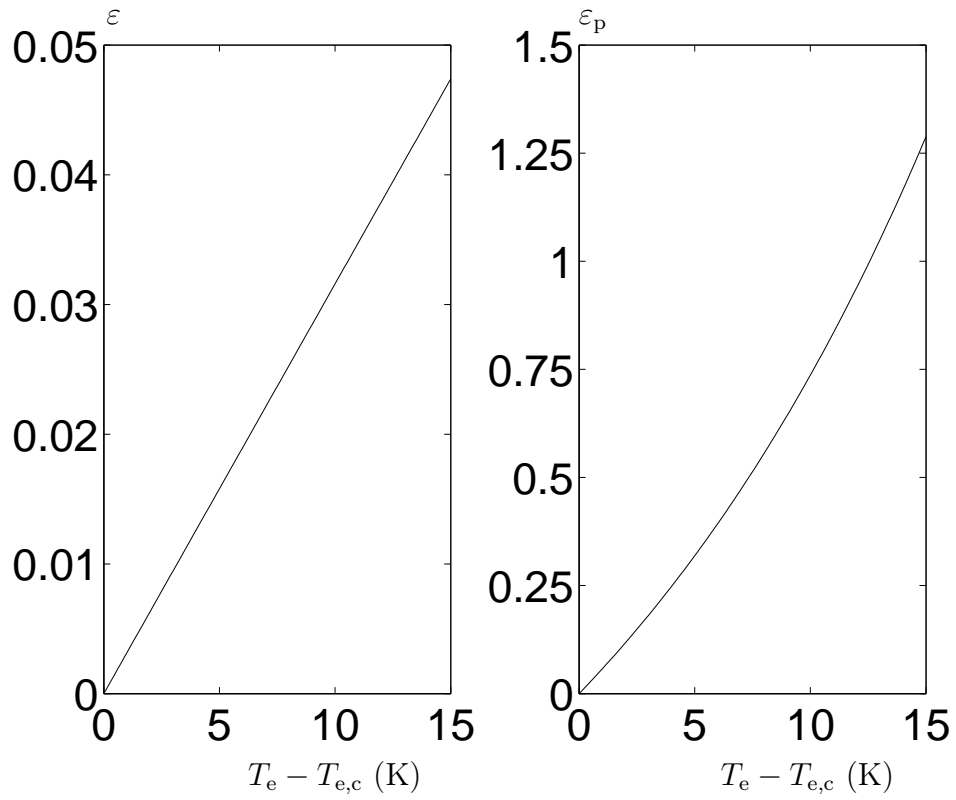
Figure 3: Control parameters as functions of $T_\mathrm{e} - T_\mathrm{e,c}$.

10

$$N^{\mathrm{T}}(f) = (\mathbf{v} \cdot \nabla \mathbf{v}, 0, \mathbf{v} \cdot \nabla \theta, 0, 0, 0, N_\theta, N_Y), \tag{16}$$

with

$$N_\theta = y_{\mathrm{v}}|_{z=1} \partial_z \theta|_{z=1}, \tag{17a}$$

$$N_Y = Y_{\mathrm{i}}(T_{\mathrm{ref,i}} + \theta\,|_{z=1}) - Y_{\mathrm{i}}(T_{\mathrm{ref,i}}) - \frac{\mathrm{d}Y_{\mathrm{i}}}{\mathrm{d}T}|_{T_{\mathrm{ref,i}}} \theta|_{z=1}; \tag{17b}$$

an upper index T means transposition, and L_ε, M, and B are linear operators with M, and B independent of the control parameter ε, contrary to L_ε. The precise definition of these operators are given in appendix A for completeness. It should be observed that the boundary conditions depending on the control parameter ε have been introduced in operator L_ε. Consequently, operator B corresponds only to boundary conditions that are independent of ε.

3   Numerical algorithms

In this section, we present successively different methods that we use later on to study the nonlinear evaporative thermoconvection. We first explain how to adapt, for this evaporation problem, the Galerkin-Eckhaus method based on a slaving principle and on an iterative algorithm needed to get convergence of the results [17, 19]. Then a finite element method and the multiple scale method are briefly discussed.

3.1   Galerkin-Eckhaus method

The Galerkin-Eckhaus method (GEM) consists first in expanding the unknown perturbation field f, satisfying Eqs. (14)-(17), in series of *eigenfunctions* of the corresponding

linear stability problem. **These expansions are introduced in the nonlinear equations.** Then this nonlinear system of equations is projected on the eigenfunctions of the adjoint linear problem and biorthogonal relations associated to this projection are used to diagonalize both the operators M and L_ε. A set of ordinary differential equations is then obtained for the *amplitudes* of the eigenfunctions [18, 19, 20]. ~~If the series expansion is truncated in an appropriate way [17], a finite set of equations can be selected to describe the system above the threshold.~~ **Using a standard slaving principle [21], which consists in reducing the infinite set of equations to a finite number by separating the set of eigenfunctions into a first set of active modes (K_a) containing modes with positive or close to zero values for the real part of the growth rate ($Re(\sigma)$), and a second set of slaved modes (K_s) containing the modes which are generated by the nonlinear growth of the active modes, which are characterized by quite negative values of $Re(\sigma)$, and whose amplitudes can be expressed as quadratic expressions of the active amplitudes, one finally obtains a finite set of amplitude equations in the active modes to describe the system above the threshold.**

Dauby et al. **[17]** have developed an iterative adaptive method to proceed toward convergence, based on the statement that the algebraic equations for the slaved modes are valid only when the amplitudes of these modes remain small enough compared to the active ones. In practice, we progressively add in K_a the slaved modes whose amplitudes are the largest with respect to the amplitudes of the active modes. This procedure is then repeated until all slaved amplitudes remain sufficiently small for the desired precision. This permits to obtain good quantitative results even far from the linear stability threshold **[17, 19]**.

It is however important to recall that the choice of an appropriate basis of eigenfunctions can be delicate, as shown recently in [19]. Due to the dependence with respect to **the control parameter** T_e of the physical parameters in the boundary conditions **(for example $\mathbf{Ma}(T_e)$ in Eq. (9))**, the eigenfunctions calculated at the **linear stability** threshold are not valuable to find a solution of the 1.5-sided model at a non zero value of the control parameter ε: the GEM solution would indeed satisfy the linearized boundary conditions evaluated at critical condition, **i.e.,** $\partial_z v + \mathbf{Ma_c}\partial_y \theta = 0$, which is incompatible with the verification of these boundary conditions at ε, **i.e.,** $\partial_z v + \mathbf{Ma}(\varepsilon)\partial_y \theta = 0$. **Contrary to the classical Marangoni-Bénard problem studied in [19],** a rescaling of the temperature, ~~so that all boundary conditions become independent of T_e, is not possible~~ **does not allow to satisfy all the boundary conditions because, for our evaporation problem,** ~~because~~ the dependence with respect to T_e appears ~~in more than one boundary condition~~ **not only in the Marangoni condition (9) but also in boundary conditions (11) and (12)**. We are thus left with the unique possibility of using the eigenfunctions calculated at ε to expand the unknown fields. On the contrary in [12, 18] the eigenfunctions were calculated at the threshold, which is **therefore** not completely correct ~~[19]~~ **as explained above**. Nevertheless, when we consider only weakly nonlinear solution at principal order in ε, as in [12, 18, 16], it can be shown that the limit of the GEM with eigenfunctions calculated at ε gives the same amplitude equations as those obtained with eigenfunctions calculated at the threshold.

Finally note that using the eigenfunctions calculated at ε to expand the unknown fields allows to satisfy only the linear boundary conditions ~~[19]~~. If the nonlinear boundary conditions (11)-(12) are to be taken into account, then the choice of an appropriate generalized eigenvalue problem seems to be unavoidable. Note that [22, 23] have investigated this possibility for a simple case of a thermal inversion problem where the generalized

13

eigenvalue problem (a Steklov problem) is known to lead to a dense expansion set. This technique has however the drawback to lead to more complicated amplitude equations and the choice of such a matrix to find an appropriate dense expansion set of eigenfunctions remains to be fully explored. For this reason, we use the linearized form of the boundary conditions when considering the GEM, i.e., we assume $N_\theta = N_Y = 0$ in (16), and verify a posteriori that this is a correct assumption. This simplifies the problem and permits to use the GEM with eigenfunctions calculated at ε.

3.2   Multiple scale and finite element methods

An alternative method to solve the nonlinear equations (14) close to the critical conditions is to use a multiple scale method (MSM) as in [19, 24, 25]. This method leads to amplitude equations as GEM. As the method consists in an asymptotic expansion with respect to the small parameter ε, it is restricted to weakly nonlinear regime. However, contrary to the GEM expansion, the nonlinear boundary conditions are naturally taken into account by MSM. We use this method at its principal order close to the critical conditions to validate our GEM results.

In the developed instability region, i.e., far from the stability threshold, we use a finite element method (FEM) to validate the iterative algorithm related to GEM slaving principle. FEM [26] is similar to GEM because it is a Galerkin method too. In FEM, a weak formulation of the problem is used that copes with the Marangoni boundary condition by considering it as a weak constraint. It consists in regarding the corresponding Lagrange multiplier as a field variable and thus to approximate it with finite boundary elements. The Femlab software is used in our computation.

4 Results

To analyze the behavior of our physical system above the convective threshold, we compare the results deduced from the three methods described above. More precisely, we consider the nonlinear evolution ~~of a stationary roll convective solution, with a wavenumber equal to the critical wavenumber k_c.~~ **with ε of a roll convective solution. In the nonlinear regime, a continuous band of wave numbers is unstable and the wavelength of the pattern typically depends on the distance to threshold. This dependence has already been studied by several authors in the past [27] and won't be considered further in the present work. Therefore, we assume in the following that the wave number of the roll pattern in the nonlinear regime remains equal to its critical value k_c.** This is a two dimensional space periodic solution of period $2\pi/k_c$ in the horizontal direction.

Let $\langle \cdot \rangle_h$ denote the horizontal average operator. Due to the periodicity of the analyzed solution, one has

$$\langle \cdot \rangle_h = (1/\lambda_c) \int_0^{\lambda_c} \cdot \, \mathrm{d}x, \tag{18}$$

with $\lambda_c = 2\pi/k_c$. To quantify the dependence with respect to the control parameter of the heat exchange between the fluid and the bottom plate, we use the Nusselt number Nu, defined as the ratio of the heat flux value at the bottom plate corresponding to the convective solution to its value for the purely conductive solution. Similarly we consider the Sherwood number Sh, which is the ratio of the evaporation rate value at the interface corresponding to the convective solution to its value for the purely conductive solution. In fact, only the horizontal average of these numbers is considered in the following, in order to obtain a global evaluation. Since both these Nusselt and Sherwood numbers increase with the control parameter, they can be considered as indicators of the convective benefits

of heat exchanges with respect to conduction. It is very interesting to note that these two numbers have the same theoretical value. The proof of this result is the following. First, the integration of the incompressibility relation (2), combined with the vanishing of the velocity at the bottom plate (6), gives $\langle w \rangle_\mathrm{h} = 0$. Then, by integrating the energy Eq. (4), we get $\langle w\theta \rangle_\mathrm{h} - \mathrm{d} \langle \theta \rangle_\mathrm{h} / \mathrm{d}z \equiv 0$, which leads to

$$\frac{\mathrm{d} \langle \theta \rangle_\mathrm{h}}{\mathrm{d}z}|_{z=1} = \frac{\mathrm{d} \langle \theta \rangle_\mathrm{h}}{\mathrm{d}z}|_{z=0} \tag{19}$$

because of the boundary conditions (6) and (8). This relation means that the horizontal averages of the heat flux are the same at the interface and at the bottom plate. Finally the interface energy conservation Eq. (10) gives the equality of Nu and Sh. This property is interesting since it can provide a necessary condition of validity and convergence of the methods used to analyze a problem.

Figure 4 is a plot of the Nusselt and Sherwood numbers in terms of the temperature T_e imposed to the system. Different curves, corresponding to the different methods, are depicted. ~~We find the same values of the Nusselt and Sherwood numbers, at a given numeric precision, for both the FEM and the GEM provided that we use a large enough set of basis functions.~~ **For the GEM, we used 41 amplitude equations (with 375 slaved modes taken into account), while 140,000 total degrees of freedom are introduced in the FEM. The agreement between the GEM and the FEM is seen to be very good.** For the MSM, only the Nusselt number is plotted because the analytical value of the Sherwood number is obviously the same ~~as the Nusselt number~~. Moreover, all the methods give the same curve slope at the critical conditions. The important result is that iterative GEM and FEM agreement is good in the non nonlinear regime when the MSM at principal order is no longer valid. The discrepancy begins
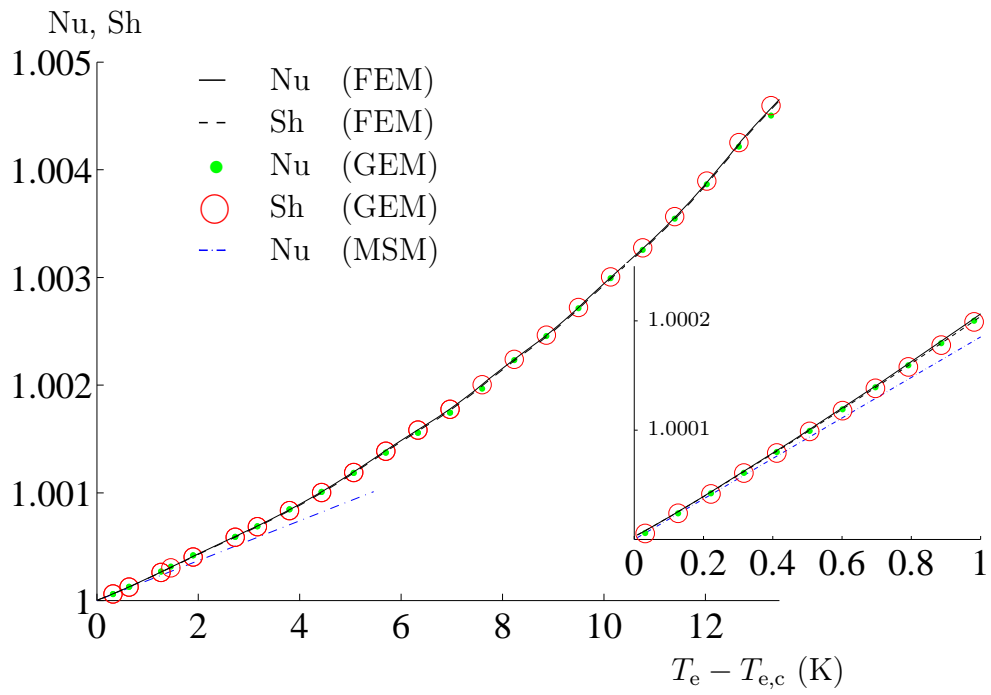
Figure 4: Nusselt and Sherwood numbers as a function of the distance to threshold (For $T_e - T_{e,c} = 12.5$ K, one has $\varepsilon = 0.041$ and $\varepsilon_p = 0.99$).

at ~~$T_e - T_{e,c} \simeq 1$. This corresponds to the control parameter value $\varepsilon = 0.003$ (or $\varepsilon_p = 0.06$).~~ $T_e - T_{e,c} \simeq 0.1$. **This corresponds to the control parameter value** $\varepsilon = 3 \times 10^{-4}$ **(or** $\varepsilon_p = 5.6 \times 10^{-3}$**).** Note also that our comparison between GEM and FEM corresponds to ε_p ranging from 0 up to 1.

Since the Nusselt and Sherwood numbers are horizontal means, it is interesting to represent the variations of several physical quantities in terms of the vertical coordinate in order to have a more complete comparison of the different nonlinear methods. To do so, note that the solution is periodic of period $2\pi/k_c$. Every scalar quantity f can thus be expressed as a Fourier series:

$$
\begin{aligned}
f = \tilde{f}_0(z) + \sum_{n=1}^{\infty} \tilde{f}_n(z) \cos(nk_c x) \\
+ \sum_{n=1}^{\infty} \hat{f}_n(z) \sin(nk_c x),
\end{aligned}
\tag{20}
$$

where $\tilde{f}_n$ and $\hat{f}_n$ are respectively **even and odd** ~~odd and even~~ modes.

In Fig. (5)-(8), some modes $\tilde{f}_n$ corresponding to several physical quantities are plotted as functions of the vertical coordinate. The non dimensional coordinate z is used in the liquid phase, while a rescaled coordinate $\tilde{z} = (H - z)/(H - 1)$ is introduced in the gas phase. We found no odd Fourier modes $\hat{f}_n$ up to $\varepsilon_p = 1$ so that these quantities are not plotted.

Figure 5 is a plot of the temperature $\tilde{\theta}_0$ and shows that the FEM results are not ~~correct very close to the critical conditions.~~ **very precise close to the threshold**. ~~This means that the convergence of FEM is more difficult to reach very close to the threshold contrary to GEM, the convergence of which is very fast close to this threshold and that is in excellent agreement with MSM. We have observed this characteristic for the simple classical Marangoni-Bénard problem without evaporation too.~~ **This is due to the fact**

that close to the bifurcation point the magnitude of the solution is very small and consequently the reduction of the many degrees of freedom to a few relevant ones, namely the order parameters given by the MSM, leads to better precision. On the contrary, the agreement between GEM and MSM is very good in the limit $\varepsilon \to 0$, which is a consequence of the theoretical equivalence of both methods in this regime (see also Fig. 6).
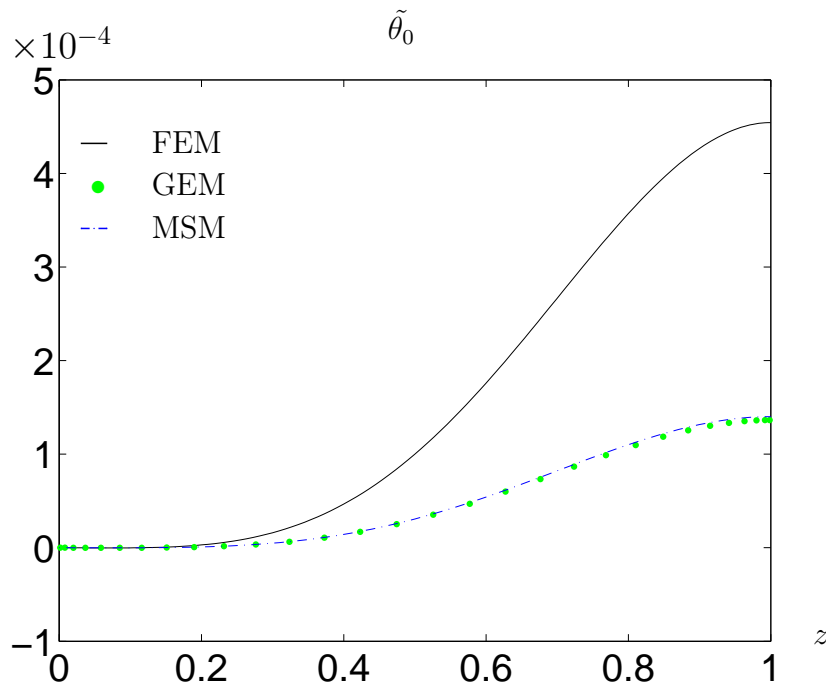

Figure 5: Comparison of temperature profiles at $T_{\mathrm{e}} - T_{\mathrm{e,c}} = 0.009$ K.

Figures 7 and 8 compare respectively the temperature, velocity, and vapor mass fraction profiles in the developed instability region, for $T_{\mathrm{e}} - T_{\mathrm{e,c}} = 2.73$ K. **We choose to plot $\tilde{\theta}_0$ and $\tilde{y}_{\mathrm{v}0}$ profiles because they are interesting mean field quantities. As the mean field velocity is obviously null, we plot $\tilde{w}_2$ velocity profile which is the first nontrivial nonlinear velocity profile close to the threshold.** The good correspondence between GEM and FEM is observed. We have verified up to $T_{\mathrm{e}} - T_{\mathrm{e,c}} = 12.5$
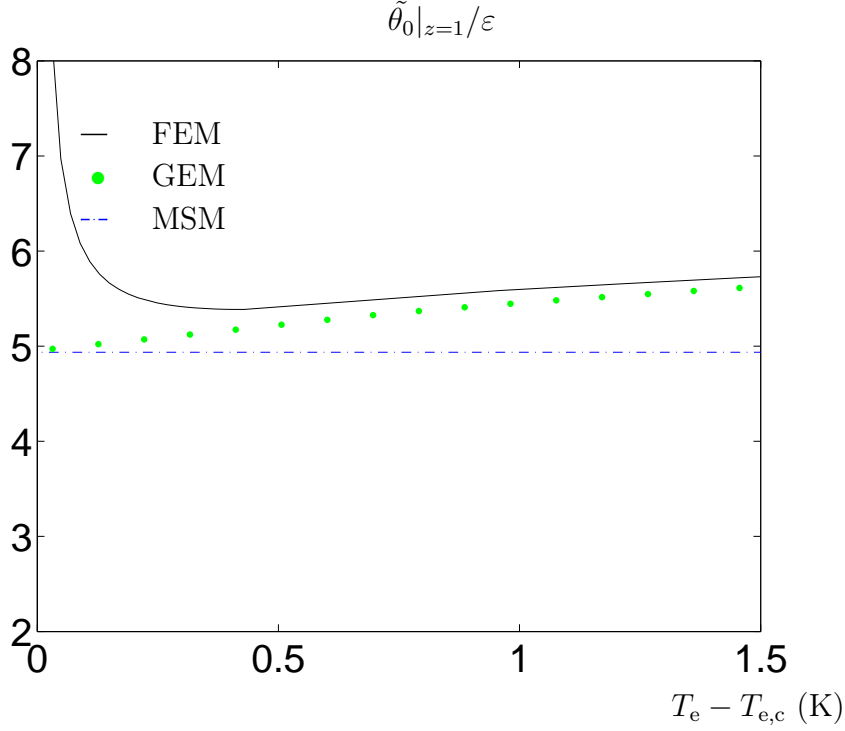
19

Figure 6: Temperature $\tilde{\theta}_0|_{z=1}/\varepsilon$ as a function of the distance to the threshold.

K that it is the case for all the other mode profiles.

Note that the description of the vapor mass fraction field (**cf. $\tilde{y}_{v1}$ profile in the gas in Fig. 8**) was a bit delicate in the FEM, due to a **thin** ~~thick~~ boundary layer which requires a fine meshing close to the liquid-gas interface.

It is important to verify that the nonlinear boundary conditions of our 1.5-sided model can be linearized. According to Eqs. (11)-(12) and (17b), it is valid to get rid of the nonlinear boundary condition terms provided that perturbations remain small, i.e.,

$$y_v|_{z=1} \ll 1 - Y_{v,ref,i}, \tag{21a}$$

$$\Theta(T_e, \theta) \ll 1, \tag{21b}$$
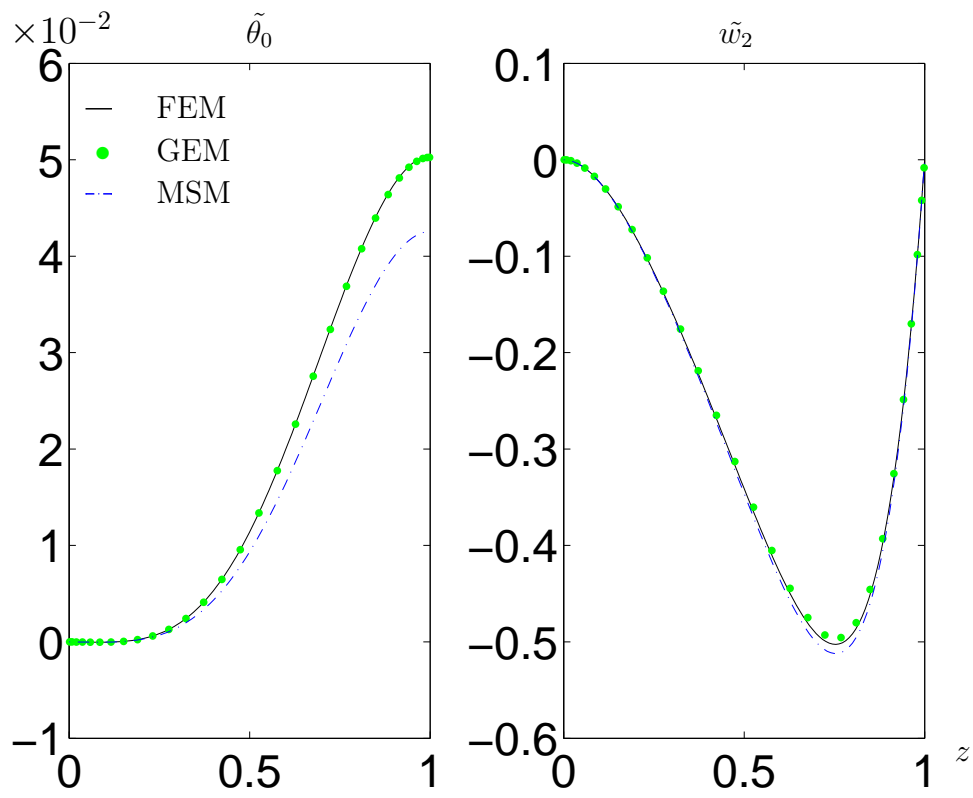
Figure 7: Comparison of temperature and velocity profiles at $T_{\mathrm{e}} - T_{\mathrm{e,c}} = 2.73$ K.
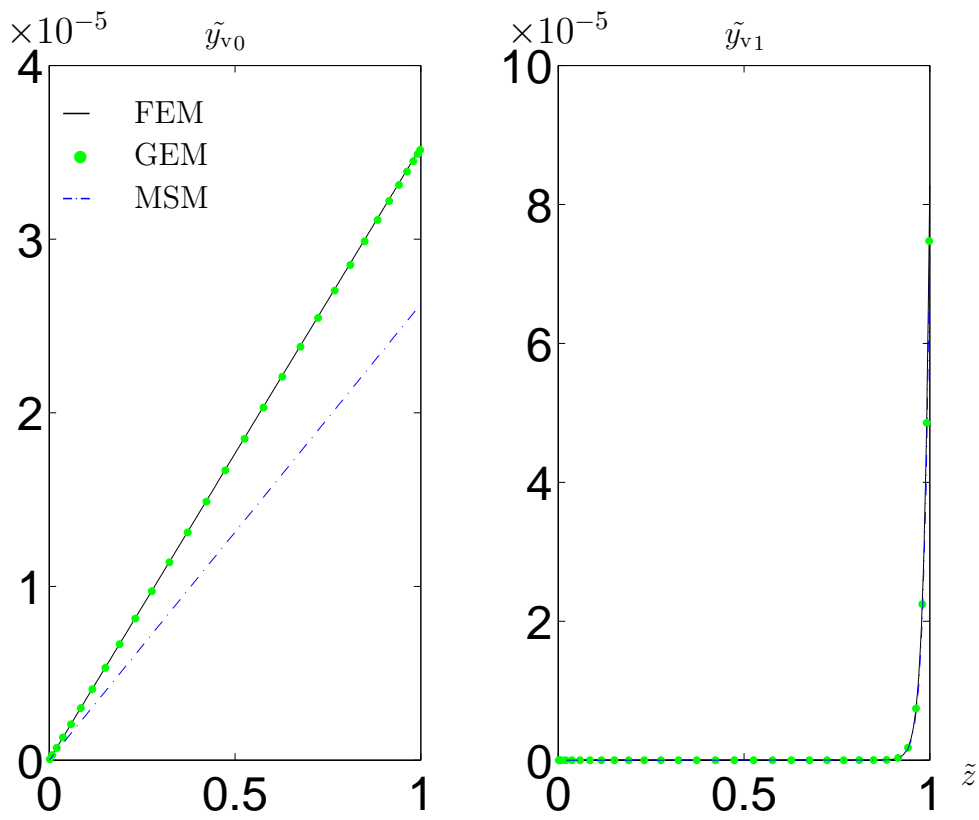
Figure 8: Comparison of vapor mass fraction profiles at $T_\mathrm{e} - T_\mathrm{e,c} = 2.73$ K.

where

$$\Theta(T_e, \theta) = N_Y / (\frac{dY_i}{dT}|_{T_{ref,i}} \theta|_{z=1}).$$

(22)

As can be shown in Fig. 9, where plot of $1 - Y_{v,ref,i}(T_e)$ and contourplot of $\Theta(T_e, \theta)$ are represented, perturbation field values must be very high for the nonlinear boundary condition terms to influence significantly the results. At $T_e - T_{e,c} = 12.5$ K, $\theta|_{z=1} \approx 0.3$ and $y_v|_{z=1} \approx 6 \times 10^{-3}$ so that relations (21) for the linearization of the boundary conditions are fulfilled.
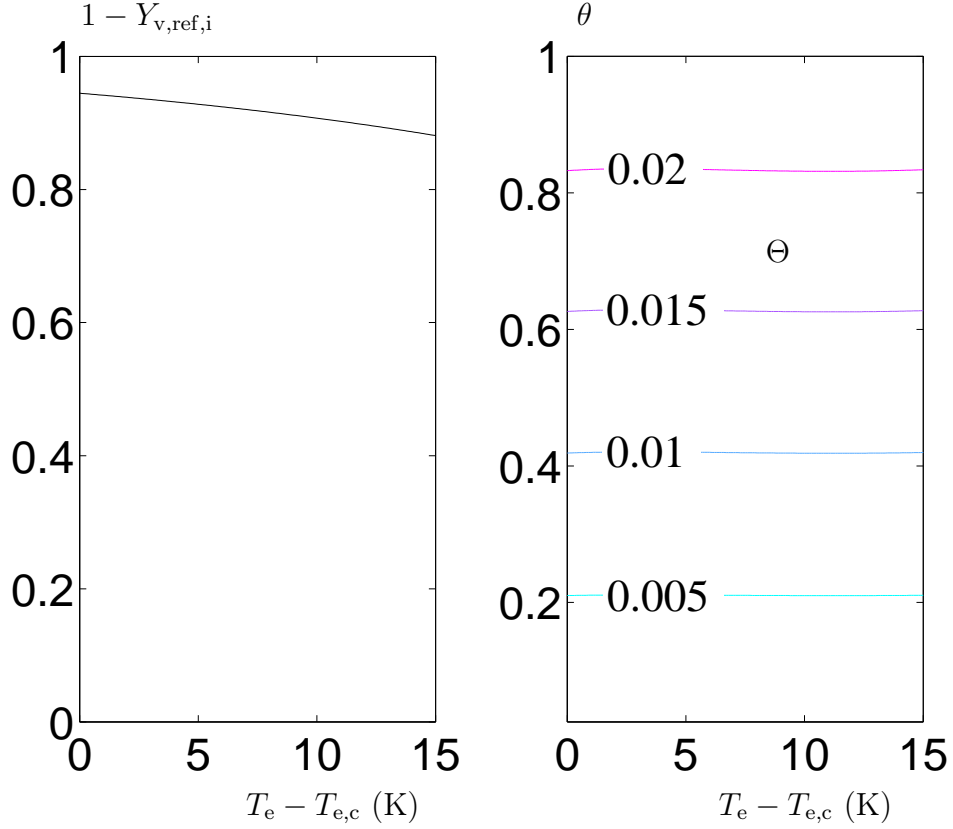

Figure 9: Validity conditions for linear boundary conditions.

As the convective solution that we have found is stationary with boundary conditions that can be linearized, Eqs. (5) and (10)-(13) are equivalent to a Biot boundary condition

that writes in Fourier space

$$\partial_z \theta + \text{Bi}_{\text{ev}}(k, T_e)\, \theta = 0 \text{ at } z = 1, \tag{23}$$

with evaporative $\text{Bi}_{\text{ev}}(k, T_e)$ expression given in [12, Eq. (55)].

Then it seems interesting and quite common [14] to consider a simple local one-sided model where the Biot number of Eq. (23) is replaced by its value with wavenumber k evaluated at k_c. Figure 10 shows however that this approximation overestimates greatly the exchange of heat at the bottom plate even in the weakly nonlinear regime. The correct solution is indeed related to the three Biot numbers corresponding to the wavenumbers 0, k_c, and $2k_c$ and it appears that $\text{Bi}_{\text{ev}}(0, T_e)$ value is very small as regard to $\text{Bi}_{\text{ev}}(k_c, T_e)$. This influences directly the mean field value and consequently the Nusselt number.
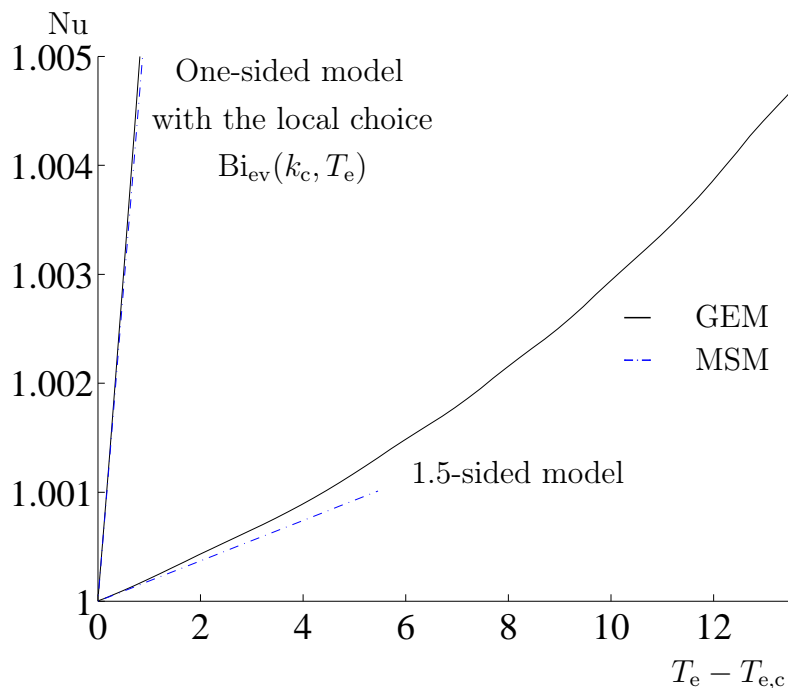

Figure 10: Local one-sided model versus 1.5-sided model.

24

5   Conclusions

Evaporative thermoconvection was studied in the nonlinear regime and the precise values of the Nusselt and Sherwood numbers were determined as functions of the distance to the threshold. The heat exchange and evaporation rate were shown to increase with the distance to threshold. Different methods were considered and a very good agreement was found between the GEM and the MSM in weakly nonlinear region. The iterative GEM algorithm was shown to give accurate results in good agreement with FEM in the developed instability domain. Finally, the one-sided model with a constant Biot number is shown to overestimate greatly the heat exchange and evaporation rate so that the importance of the 1.5-sided model is brought to light.

It would be very interesting to use the same GEM iterative algorithm to obtain precise quantitative three dimensional space stationary solutions so as to derive quantitative **amplitude and phase** stability diagrams **considering both** (x, y) **pattern selection and wavenumber selection**.

Appendix A. Definition of operators L_ε, M, and B

For the sake of completeness, we give here the definitions of the operators that were introduced in section 2:

$$
L_\varepsilon =
\begin{pmatrix}
\mathrm{Pr}\nabla^2 & -\nabla & \mathrm{Pr}\mathrm{Ra}\mathbf{e}_z & \cdots & \cdots & \cdots & \cdots & \cdots \\
\nabla\cdot & \cdots & \cdots & \cdots & \cdots & \cdots & \cdots & \cdots \\
(T_\mathrm{e}-T_\mathrm{ref,i})(\cdot)\cdot\mathbf{e}_z & \cdots & \nabla^2 & \cdots & \cdots & \cdots & \cdots & \cdots \\
\cdots & \cdots & \cdots & \frac{\kappa}{\mathrm{Le}}\nabla^2 & \cdots & \cdots & \cdots & \cdots \\
-\partial_z(\cdot)\cdot\mathbf{e}_x|_{z=1} & \cdots & -\mathrm{Ma}\partial_x(\cdot)|_{z=1} & \cdots & \cdots & \cdots & \cdots & \cdots \\
-\partial_z(\cdot)\cdot\mathbf{e}_y|_{z=1} & \cdots & -\mathrm{Ma}\partial_y(\cdot)|_{z=1} & \cdots & \cdots & \cdots & \cdots & \cdots \\
\cdots & \cdots & (1-Y_\mathrm{v,ref,i})\partial_z(\cdot)|_{z=1} & \begin{pmatrix} J_\mathrm{ref}(\cdot)|_{z=1} \\ -\frac{\rho\kappa}{\mathrm{Le}}\partial_z(\cdot)|_{z=1} \end{pmatrix} & \cdots & \cdots & \cdots & \cdots \\
\cdots & \cdots & -\frac{\mathrm{d}Y_\mathrm{i}}{\mathrm{d}T}|_{T_\mathrm{ref,i}}(\cdot)|_{z=1} & (\cdot)|_{z=1} & \cdots & \cdots & \cdots & \cdots
\end{pmatrix},
\tag{24}
$$

$$
M =
\begin{pmatrix}
1 & \cdots & \cdots & \cdots & \cdots & \cdots & \cdots & \cdots \\
\cdots & \cdots & \cdots & \cdots & \cdots & \cdots & \cdots & \cdots \\
\cdots & \cdots & 1 & \cdots & \cdots & \cdots & \cdots & \cdots \\
\cdots & \cdots & \cdots & 1 & \cdots & \cdots & \cdots & \cdots \\
\cdots & \cdots & \cdots & \cdots & \cdots & \cdots & \cdots & \cdots \\
\cdots & \cdots & \cdots & \cdots & \cdots & \cdots & \cdots & \cdots \\
\cdots & \cdots & \cdots & \cdots & \cdots & \cdots & \cdots & \cdots \\
\cdots & \cdots & \cdots & \cdots & \cdots & \cdots & \cdots & \cdots
\end{pmatrix},
\tag{25}
$$

and

$$
B = \begin{pmatrix}
(\cdot)|_{z=0} & \cdots & \cdots & \cdots & \cdots & \cdots & \cdots & \cdots \\
\cdots & \cdots & (\cdot)|_{z=0} & \cdots & \cdots & \cdots & \cdots & \cdots \\
\cdots & \cdots & \cdots & (\cdot)|_{z=H} & \cdots & \cdots & \cdots & \cdots \\
(\cdot) \cdot \mathbf{e}_z|_{z=1} & \cdots & \cdots & \cdots & \cdots & \cdots & \cdots & \cdots
\end{pmatrix} . \tag{26}
$$

References

[1] J.C. Berg, M. Boudart, A. Acrivos, J. Fluid Mech. 24 (1966) 721.

[2] P. Colinet, L. Joannes, C.S. Iorio, B. Haut, M. Bestehorn, G. Lebon, J.C. Legros, Adv. Space Res. 32 (2003) 119.

[3] H. Mancini, D. Maza, Europhys. Lett. 66 (6) (2004) 812–818.

[4] J.P. Burelbach, S.G. Bankoff, S.H. Davis, J.Fluid Mech. 195 (1988) 463.

[5] V. Ha, C. Lai, J. Chin. Inst. Eng. 21 (1998) 547.

[6] P. Colinet, B. Haut, J. Margerit, F. Peeters, J.C. Legros, G. Lebon, V. Halloin, in: Proc. of CHISA 2002, 15th International Congress of Chemical and Process Engineering, CD-ROM Paper 858.

[7] B. Haut, P. Colinet, J. Colloid Interface Sci. 285 (2005) 296–305.

[8] J. Margerit, G. Lebon, P. Colinet, C.S. Iorio, J.C. Legros, Phys. Rev. E 68 (2003) 041601.

[9] C. Moussy, G. Lebon, J. Margerit, Eur. Phys. J. B 40 (2004) 327–335.

[10] R. Borcia, M. Bestehorn, Eur. Phys. J. B 44 (2005) 101–108.

[11] M. Dondlinger, J. Margerit, P.C. Dauby, J. Colloid Interface Sci. 283 (2) (2005) 522–532.

[12] J. Margerit, M. Dondlinger, P.C. Dauby, J. Colloid Interface Sci. 290 (1) (2005) 920–930.

[13] E. Sultan, A. Boudaoud, M. B. Amar, J. Fluid Mech. 543 (2005) 183–202.

[14] D. Merkt, M. Bestehorn, Physica D 185 (2003) 196.

[15] O. Ozen, R. Narayanan, Phys. Fluids 16 (12) (2004) 4653–4660.

[16] B. Echebarria, C. Pérez-García, Phys. Rev. E 63 (2001) 066307.

[17] P.C. Dauby, T. Desaive, J. Bragard, P. Cerisier, Phys. Rev. E 64 (2001) 066301.

[18] P.M. Parmentier, V.C. Regnier, G. Lebon, J.C. Legros, Phys. Rev. E 54 (1996) 411.

[19] M. Dondlinger, J. Margerit, P.C. Dauby, under consideration **for publication**.

[20] W. Eckhaus, Studies in Non-Linear Stability Theory, Springer Verlag, New York, 1965.

[21] P. Manneville, Dissipative Structures and Weak Turbulence, Academic Press, Inc., 1990.

[22] O. Quemener, J. Battaglia, A. Neveu, Int. J. Therm. Sci. 42 (4) (2003) 361–378.

[23] A. Neveu, K. El-Khoury, B. Flament, Int. J. Therm. Sci. 38 (4) (1999) 289–304.

[24] W.V.R. Malkus, G. Veronis, Finite amplitude cellular convection, J. Fluid Mech. 4 (1958) 225–260.

[25] J. Bragard, M.G. Velarde, J. Fluid Mech. 368 (1998) 165–194.

[26] O. Pironneau, Finite element methods for fluids, John Wiley & Sons, 1989.

[27] P. Colinet, J.C. Legros, M.G. Velarde, Nonlinear Dynamics of Surface Tension Driven Instabilities, Wiley-VCH, Berlin, 2001.